
MISSING DATA AS AUGMENTATION IN THE EARTH OBSERVATION DOMAIN: A MULTI-VIEW LEARNING APPROACH

A PREPRINT

Francisco Mena^{1,2} , Diego Arenas² , Andreas Dengel^{1,2} 

¹Department of Computer Science, University of Kaiserslautern-Landau (RPTU), Germany;

²SDS, German Research Center for Artificial Intelligence (DFKI), Germany.

f.menat@rptu.de, {diego.arenas, andreas.dengel}@dfki.de

ABSTRACT

Multi-view learning (MVL) leverages multiple sources or views of data to enhance machine learning model performance and robustness. This approach has been successfully used in the Earth Observation (EO) domain, where views have a heterogeneous nature and can be affected by missing data. Despite the negative effect that missing data has on model predictions, the ML literature has used it as an augmentation technique to improve model generalization, like masking the input data. Inspired by this, we introduce novel methods for EO applications tailored to MVL with missing views. Our methods integrate the combination of a set to simulate all combinations of missing views as different training samples. Instead of replacing missing data with a numerical value, we use dynamic merge functions, like average, and more complex ones like Transformer. This allows the MVL model to entirely ignore the missing views, enhancing its predictive robustness. We experiment on four EO datasets with temporal and static views, including state-of-the-art methods from the EO domain. The results indicate that our methods improve model robustness under conditions of moderate missingness, and improve the predictive performance when all views are present. The proposed methods offer a single adaptive solution to operate effectively with any combination of available views.

Keywords Multi-view Learning, Earth Observation, Missing Data, Data Augmentation, Robustness.

1 Introduction

Nowadays, the usage of multiple data sources, sensors, or views in ML models has become a standard practice in various applications and domains [Yan et al., 2021]. The reason is that by using multiple sources of information, the individual data can be ratified and complemented to enhance predictive models [Hong et al., 2021, Sainte Fare Garnot et al., 2022]. Earth Observation (EO) is one of the domains where Multi-View Learning (MVL) has been used to provide comprehensive insights in various applications [Mena et al., 2024c]. In our work, we refer to a *view* as all features in a specific data source. For example, a view can be an optical or radar Satellite Image Time Series (SITS), weather conditions, topographic information, or various metadata, consisting of a heterogeneous scenario with different spatio-temporal resolutions. Thus, there are *temporal views*, with multi-temporal data and *static views*, with single-date data. This diversity distinguishes research done in EO from other ML domains such as vision and text [Rolf et al., 2024]. Furthermore, EO views might not be a persistent source of information as researchers commonly assume.

The EO domain faces challenges due to the finite lifespan of remote sensors, noise, and cloudy conditions in optical sensors [Shen et al., 2015]. Besides, unexpected errors can affect the availability of the data, such as the failure of the Sentinel-1B satellite in 2021. This problem leads to scenarios with missing data, which hinder accurate predictions and introduce biases in ML models [Choi and Lee, 2019, Hong et al., 2021, Sainte Fare Garnot et al., 2022]. For instance, [Mena et al., 2024a] evidence the negative predictive impact that missing views have in different vegetation applications, highlighting the lack of robustness of different MVL models. Even current ML models, like Transformers, are not naturally robust to missing views [Ma et al., 2022, Tseng et al., 2023, Chen et al., 2024]. This leaves open questions such as how to increase the robustness of MVL models to missing views.

Despite the negative impact of missing data in ML models, many studies actively incorporate it during learning. For instance, it has been used as a masking operator for self-supervision in text [Devlin et al., 2018], signal [Cao et al., 2018] and vision domains [He et al., 2022]. Another option is to use Missing data as Augmentation (MAug) techniques, such as the dropout layer [Srivastava et al., 2014], and augmentation operations in the vision domain (e.g. crop). In the EO domain, the MAug technique has been used in MVL models. One case is to drop all features from a random view (sensor) during training [Wang et al., 2022, Mena et al., 2024b]. Another case corresponds to including all combinations of missing views, as experimented by [Gawlikowski et al., 2023] in out-of-distribution detection. However, most of these works use a fixed-size merge function (like concatenation) and validate on EO datasets with only static views.

In this work, we introduce methods based on two main components, all Combinations of Missing views (CoM) and a dynamic merge function at feature-level. The CoM acts as an augmentation technique, simulating all combinations of missing views in the training set, which relates to literature [Gawlikowski et al., 2023, Mena et al., 2024b]. However, we apply the MAug technique at the feature-level instead of at the input [Mena et al., 2024b] and use dynamic merge instead of fixed functions [Gawlikowski et al., 2023]. We find that integrating the CoM with a merge function that ignores the missing views enhances the predictions and robustness of MVL models. The dynamic merge can be a simple average or a more complex function. Inspired by literature on using ML models as aggregators [Lee et al., 2019, Bagueño and Mendoza, 2020, Wang et al., 2021, Guo et al., 2024], we include some alternative functions based on gated fusion, cross-attention fusion, and memory fusion.

We validate the proposed methods on four EO datasets with temporal and static views, and compare them to five state-of-the-art methods in the EO domain. For assessing the robustness to missing data, we simulate missing views during inference and compare the predictions to full-view data. The evidence suggests that our methods have better robustness than competing methods in cases of moderate missingness, and in some cases improve predictive performance when all views are available.

Overall, our main contributions are as follows: i) we propose a MAug technique tailored to missing views in MVL at feature level (CoM), ii) adapt the MAug technique to ignore the features of the missing views by using a dynamic fusion, and iii) validate on EO datasets with classification and regression tasks, considering temporal and static views. The proposed methods, inspired by sensor invariant modeling [Francis, 2024, Mena et al., 2024b], allow a model to generate adaptive predictions based on the available views. Our code will be released at <https://github.com/fmenat/com-views>.

2 Related work

MVL with EO data. Recently, there has been an increase in EO research using multiple data sources to enhance ML model predictions [Camps-Valls et al., 2021]. The main difference in the MVL models investigated is how the data is fused [Mena et al., 2024c]. Input-level fusion has been the common choice for this, i.e. merge the data before feeding a ML model. For instance, [Kussul et al., 2017] feed a CNN model with just the concatenation of different sensors (multi-spectral and radar images) for land-use classification, while [Ghamisi et al., 2016] concatenate specialized hand-crafted features from hyper-spectral and LiDAR images. However, several works have shown that learning view-dedicated feature extractors (encoders) improves results [Hong et al., 2021, Sainte Fare Garnot et al., 2022, Ferrari et al., 2023, Mena et al., 2024d]. For example, [Audebert et al., 2018] propose a MVL model for multi-spectral and topographic images that fuses across multiple layers of CNN encoders. Later, [Zhang et al., 2020] show that including a fusion in the decision layer (as a hybrid fusion) improves the results for land-use segmentation. Additionally, [Ofori-Ampofo et al., 2021] evidence that using specialized encoder architectures for optical and radar SITS benefits the feature-level fusion in a crop-type classification use-case. Furthermore, there have been efforts in exploring geospatial foundational models using multi-view data. For instance, Presto [Tseng et al., 2023] uses an input-level fusion with a Transformer model, while SkySense [Guo et al., 2024] uses a feature-level fusion based on view-dedicated models that are fine-tuned based on the available views in the downstream tasks.

Missing data in EO applications Different forms of missing (such as errors and anomalies) are present in EO data [Shen et al., 2015]. As expected, when the missing information in the input data increases (at spectral, spatial, or temporal dimensions), the predictions of ML models get worse [Fasnacht et al., 2020, Ofori-Ampofo et al., 2021, Ebel et al., 2023]. In addition, specific data sources are more relevant than others. For example, the lack of an optical view critically affects models’ accuracy [Hong et al., 2021, Mena et al., 2024a]. Nevertheless, there is evidence that when a view is missing, training with additional views can supplement and increase the model robustness [Inglada et al., 2016, Hong et al., 2021]. For instance, [Ferrari et al., 2023] and [Sainte Fare Garnot et al., 2022] show that when optical images are missing in SITS due to cloudy conditions, placing the fusion far away from the input layer increases the model robustness. Furthermore, in [Mena et al., 2024a] three techniques that mitigate the effect of missing views in MVL are compared. The first is to impute the missing view with a numerical value. The second

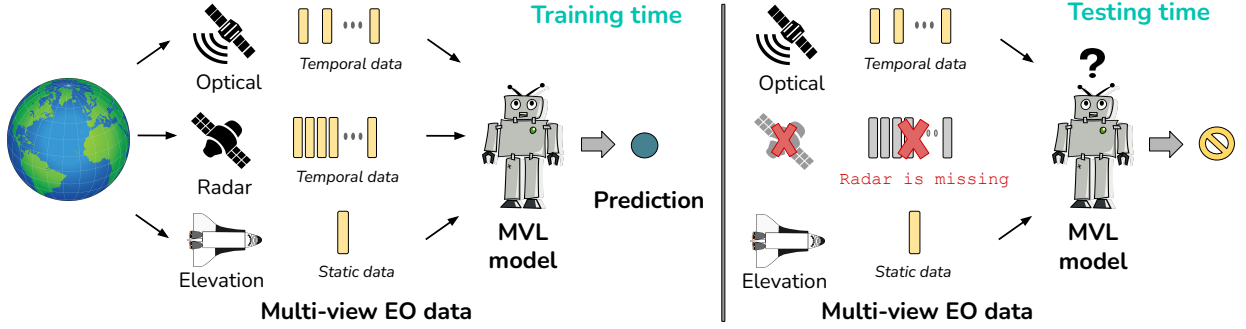


Figure 1: Illustration of a MVL scenario with three views available during training, while at inference time, one view is missing.

replaces the missing view with a similar sample in the training set. The last one ignores the missing views in the aggregation through a dynamic fusion. The latter is the technique that has shown greater robustness in various EO datasets when views are missing [Mena et al., 2024a], as well when images are missing in SITS [Che et al., 2024]. Furthermore, modifying model components can also increase predictive robustness, as has been shown when sharing layer weights [Zheng et al., 2021, Mena et al., 2024b].

Leverage missing data Simulate missing data has been progressively used in ML research, from standard augmentation techniques (MAug) in the vision domain (like crops) to masking out image patches for reconstruction, as a self-supervised framework [He et al., 2022]. In the natural language domain, it has been used to learn token embeddings from reconstruction tasks [Devlin et al., 2018]. In the signal domain, it has been studied how to best impute data in time series [Cao et al., 2018, Du et al., 2023]. In the EO domain, masking out input data and learning to reconstruct it has been widely used for self-supervised learning, such as in SatMAE [Cong et al., 2022], SITS-Former [Yuan et al., 2022], Presto [Tseng et al., 2023], and OmniSat [Astruc et al., 2025]. Similarly, the dropout operator has not only considered data augmentation [Bouthillier et al., 2015] but used as such. For instance, [Fasnacht et al., 2020] introduce a spectral dropout to increase the model robustness to missing spectral bands for hyper-spectral image segmentation. In the same predictive task, [Haut et al., 2019] use spatial dropout (random occlusion) as a MAug technique. Furthermore, randomly dropping images in SITS, i.e. Temporal Dropout (TempD), has been presented as an effective MAug technique for prediction [Sainte Fare Garnot et al., 2022]. Recently, the MAug has been applied to sensors, i.e. Sensor Dropout (SensD), as a way to learn inter-sensor representations [Wang et al., 2022], to avoid overfitting to dominant sensors [Chen et al., 2024], to assess sensors contribution [Ekim and Schmitt, 2024], and to increase model robustness to missing data [Mena et al., 2024b]. Additionally, [Gawlikowski et al., 2023] show that the MAug applied to views can be used for out-of-distribution detection in two-view image classification tasks.

Most of the works that use the concept of MAug in EO focus on masking out the data at the input-level or using a fixed merge function. In practice, this means imputing the missing features with a *fake* value to obtain a fixed-size input in all scenarios. Moreover, the literature positions the input-level as a fusion strategy with low predictive capacity and robustness. To overcome these disadvantages, our work focuses on using a MAug at feature-level by ignoring the missing views in the MVL model. We achieve this by using dynamic merge functions, as we show below.

3 Multi-view learning with missing data

3.1 Problem notation

Given the multi-view input data for a sample i , $\mathcal{X}^{(i)} = \{\mathcal{X}_v^{(i)}\}_{v \in \mathcal{V}}$, with \mathcal{V} the set of all views, the objective is to find a MVL model $\mathcal{G}(\cdot)$ that approximates the corresponding target $y^{(i)}$, i.e. $\hat{y}^{(i)} = \mathcal{G}(\mathcal{X}^{(i)})$. The views \mathcal{X}_v can be temporal (time-series data) or static (single-date data). The learning is through minimizing a loss function of the form $\mathcal{L}(y^{(i)}, \mathcal{G}(\mathcal{X}^{(i)}))$, over a training set of N samples, $\mathcal{D} = \{\mathcal{X}^{(i)}, y^{(i)}\}_{i=1}^N$. In the case of missing views, instead, we observe $\tilde{\mathcal{X}}^{(i)} = \{\mathcal{X}_v^{(i)}\}_{v \in \mathcal{V}^{(i)}}$, with $\mathcal{V}^{(i)} \subseteq \mathcal{V}$, the set of available views for a sample i . Then, the number of views is $m = |\mathcal{V}|$ and $m^{(i)} = |\mathcal{V}^{(i)}|$, with $m^{(i)} > 0$. As views in MVL models could be any set of features, we consider a view as all features from a data source (e.g. optical, radar, weather). We consider a full-view training scenario, with expected missing views at inference, as illustrated in Figure 1.

3.2 Basis of multi-view learning

Input-level fusion This fusion strategy directly merges the input features of the views. As EO views have different (spatio-temporal) resolutions, an alignment step is required to match all the dimensions: $\mathcal{X}_F^{(i)} = \text{concat}(\text{alignment}(\mathcal{X}^{(i)}))$. Then, these merged features are fed to a single ML model: $\hat{y}^{(i)} = \mathcal{G}(\mathcal{X}_F^{(i)})$. However, in this fusion strategy, there is no clear way to deal with missing views, $\tilde{\mathcal{X}}^{(i)}$. For instance, [Hong et al., 2021] present a zero-imputation of the missing data, i.e. $\mathcal{X}^{(i)} = \tilde{\mathcal{X}}^{(i)} \cup \{\mathbf{0}\}_{v \in \mathcal{V} \setminus \mathcal{V}^{(i)}}$. Subsequent research on MAug has used the zero-imputation in the missing features [Gawlikowski et al., 2023, Mena et al., 2024b], i.e. augment the training data by masking out views with a zero value. Nonetheless, zero is an arbitrary value that creates bias depending on data normalization and transformations applied.

Feature-level fusion To avoid forcing a view-alignment, and have a single model that handles the multi-view information, this strategy extracts high-level features through view-dedicated encoders: $\mathbf{z}_v^{(i)} = \mathcal{G}_v^{\text{enc}}(\mathcal{X}_v^{(i)}) \forall v \in \mathcal{V}$. In addition, a normalization layer (with learnable parameters) is used in each encoder to scale and harmonize the different representations. Then, a merge function combines this information, obtaining a joint representation, $\mathbf{z}_F^{(i)} = \mathcal{M}(\{\mathbf{z}_v^{(i)}\}_{v \in \mathcal{V}})$. The merge function $\mathcal{M}(\cdot)$ can take any form, such as concatenation or dynamic functions. Then, a prediction head is used to obtain the final prediction: $\hat{y}^{(i)} = \mathcal{G}^{\text{head}}(\mathbf{z}_F^{(i)})$. In the following, we explain how to handle missing views in the latter fusion strategy.

3.3 Dynamic feature-level fusion

Inspired by permutation [Lee et al., 2019] and sensor [Francis, 2024, Mena et al., 2024b] invariant models, we rely on ignoring the encoded features associated to the missing views. For this, the MVL model encodes and merges only the available views:

$$\mathbf{z}_v^{(i)} = \mathcal{G}_v^{\text{enc}}(\mathcal{X}_v^{(i)}) \quad \forall v \in \mathcal{V}^{(i)}, \quad (1)$$

$$\mathbf{z}_F^{(i)} = \mathcal{M}\left(\left\{\mathbf{z}_v^{(i)}\right\}_{v \in \mathcal{V}^{(i)}}\right), \quad (2)$$

with $\mathbf{z}_v^{(i)} \in \mathbb{R}^d$ and $\mathbf{z}_F^{(i)} \in \mathbb{R}^{d^F}$. However, when the fused dimension (d^F) depends on the number of views ($m^{(i)}$), as with concatenation, fusion cannot be dynamic. Thus, we use merge functions that yield the same fused dimension regardless of the fused views, i.e. $d^F = d$. We call these dynamic merge functions. A simple case is a linear combination with the same weight, i.e. average as

$$\mathcal{M}\left(\mathbf{Z}^{(i)}\right) = \frac{1}{m^{(i)}} \sum_{v \in \mathcal{V}^{(i)}} \mathbf{z}_v^{(i)}. \quad (3)$$

Furthermore, we present some alternatives in the following.

Gated fusion Instead of using the same weight for all views as in the average, we use a data-driven weighted fusion [Choi and Lee, 2019, Mena et al., 2024d]. Considering the encoded features from all views as $\mathbf{Z}^{(i)} = \text{stack}(\{\mathbf{z}_v^{(i)}\}_{v \in \mathcal{V}}) \in \mathbb{R}^{m \times d}$, the gated merge function is expressed by

$$\mathcal{M}\left(\mathbf{Z}^{(i)}\right) = \sum_{v \in \mathcal{V}} \text{softmax}\left(\mathbf{A}^{(i)}\right)_v^\top \odot \mathbf{Z}_v^{(i)}, \quad (4)$$

with $\mathbf{A}^{(i)}$ the fusion weights. Then, instead of modeling a single fusion weight for all dimensions d in each view, $\mathbf{A}^{(i)} \in \mathbb{R}^{1 \times m}$ [Mena et al., 2024d], we use a per-dimension weight in each view, i.e. $\mathbf{A}^{(i)} \in \mathbb{R}^{d \times m}$, calculated as

$$\mathbf{A}^{(i)} = W_G \cdot \text{flatten}\left(\mathbf{Z}^{(i)}\right) + \mathbf{b}, \quad (5)$$

with W_G and \mathbf{b} learnable parameters. In the case of missing data, the fusion weights of the unavailable views are modified, such as $\text{softmax}(\mathbf{A}^{(i)})_v = \mathbf{0} \forall v \in \mathcal{V} \setminus \mathcal{V}^{(i)}$. With this adaptation of weights, the features of the missing views are ignored in the merge Eq. (4). As the fusion weights require all views to be calculated, Eq. (5), and we only forward over the available views, Eq. (1), during implementation we impute the missing features with zeros, $\mathbf{z}_v^{(i)} = \mathbf{0} \forall v \in \mathcal{V} \setminus \mathcal{V}^{(i)}$.

Cross-attention fusion Inspired by Transformer layers used to fuse EO data [Ma et al., 2022, Chen et al., 2024], we use a learnable parameter, called *fusion token*, $\mathbf{f} \in \mathbb{R}^d$ to query the multi-view data. Consider the encoded features from the available views with the fusion token as $\mathbf{Z}^{(i)} = \text{stack}(\mathbf{f}, \{\mathbf{z}_v^{(i)}\}_{v \in \mathcal{V}^{(i)}}) \in \mathbb{R}^{(1+m^{(i)}) \times d}$, the cross-attention merge function is expressed by

$$\mathcal{M}(\mathbf{Z}^{(i)}) = \text{softmax}(\mathbf{A}^{(i)})_0 \cdot \mathbf{Z}^{(i)} \mathbf{W}_V, \quad (6)$$

with $\mathbf{A}^{(i)} \in \mathbb{R}^{(1+m^{(i)}) \times (1+m^{(i)})}$ the cross-view (and token) attention weights, and \mathbf{W}_V a learnable parameter. The values $\mathbf{A}_0^{(i)} \in \mathbb{R}^{1 \times (1+m^{(i)})}$ are the view-attention weights of the fusion token used to aggregate the views. These weights are computed by a self-attention mechanism as follows

$$\mathbf{A}^{(i)} = \mathbf{Z}^{(i)} \mathbf{W}_Q \cdot \mathbf{Z}^{(i)} \mathbf{W}_K + \mathbf{b}, \quad (7)$$

with \mathbf{W}_Q , \mathbf{W}_K , and \mathbf{b} learnable parameters. As the matrix computation in Eq. (7) depends exclusively on the available views, the model naturally avoids attending the missing views when merging Eq. (6), i.e. $\mathbf{A}_v^{(i)} = \mathbf{0} \quad \forall v \in \mathcal{V} \setminus \mathcal{V}^{(i)}$. We use a multi-head mechanism and stacked layers to increase the learning of cross-view features [Vaswani et al., 2017]. In contrast to previous works [Lee et al., 2019, Chen et al., 2024], we include a view-specific positional encoding.

Memory fusion Inspired by RNN models used to fuse multi-view EO data [Wang et al., 2021], we employ a memory-based fusion. The memory is updated one view at a time with an empty initial memory, expressed by

$$\mathbf{h}_v^{(i)} = \mathcal{R}(\mathbf{z}_v^{(i)}, \mathbf{h}_{v-1}^{(i)}) \quad \mathbf{h}_0 = \mathbf{0}, \quad (8)$$

with \mathcal{R} a RNN model, and $v \in \{1, \dots, m^{(i)}\}$. Then, the memory-based fused vector corresponds to $\mathcal{M}(\{\mathbf{z}_v^{(i)}\}_{v \in \mathcal{V}^{(i)}}) = \mathbf{h}_{m^{(i)}}^{(i)}$. This means that the fused vector is the memory (or hidden state in the RNN model) after being recursively updated with all views. As the recursive operation Eq. (8) and fused vector is invariant to the number of views given as input, it naturally ignores missing views. Similar to the cross-attention fusion, we stack multiple LSTM layers in $\mathcal{R}(\cdot)$ to increase the learning of cross-view features. Since RNNs are order-dependent, a random permutation can be used to avoid a bias in the order in which the views are given. However, using the proposed MAug technique is enough for generalization, as shown in the appendix.

3.4 All combinations of missing views

As previous works have shown, randomly dropping views during training increases the model robustness to missing views [Tseng et al., 2023, Chen et al., 2024]. However, it can negatively affect the model accuracy in the full-view scenario [Mena et al., 2024b]. Thus, we consider augmenting the training samples by modeling all combinations of missing views at feature-level. Then, assuming a full-view training set, the augmented features extracted from the i -th sample are $\{\{\mathbf{z}_v^{(i)}\}_{v \in \mathcal{V}^{(j)}}\}_{\mathcal{V}^{(j)} \in \mathcal{T}}$, with $\mathcal{T} = \{\mathcal{V}^{(j)} : \mathcal{V}^{(j)} \subseteq \mathcal{V}, \mathcal{V}^{(j)} \neq \emptyset\}$ the augmented list. Here, the number of possible combinations is the same as the power set of \mathcal{V} minus the no-view case, i.e. $|\mathcal{T}| = 2^m - 1$. For instance, for optical, radar, and weather views, the augmented list is $\mathcal{T} = \{(\text{optical}/\text{radar}/\text{weather}), (\text{optical}/\text{radar}), (\text{optical}/\text{weather}), (\text{radar}/\text{weather}), (\text{optical}), (\text{radar}), (\text{weather})\}$. We named this MAug technique as **Combinations of Missing views (CoM)**. The usage of CoM during training is illustrated in Algorithm 1.

We consider a balanced contribution between the full-view and missing views predictive performance. This means that all augmented samples from \mathcal{T} have the same weight in the loss function during training, expressed by

$$\ell = \frac{1}{N} \sum_{i=1}^N \frac{1}{|\mathcal{T}|} \sum_{\mathcal{V}^{(j)} \in \mathcal{T}} \mathcal{L}(y^{(i)}, \hat{y}_j^{(i)}), \quad (9)$$

with $\hat{y}_j^{(i)} = \mathcal{G}(\{\mathbf{X}_v^{(i)}\}_{v \in \mathcal{V}^{(i)}})$. Furthermore, to reduce computational operations of the multiple predictions, we forward over the encoders (biggest computation bottleneck) only once, while the fusion and prediction are done $|\mathcal{T}|$ times, see Algorithm 1 for details.

4 Experiments

4.1 Datasets

We use the following pixel-wise EO datasets with static and temporal views. More details on the feature description can be found in A.1.

Algorithm 1 CoM technique at feature-level**Input:** $\mathcal{D} : \{\mathcal{X}^{(i)}, y^{(i)}\}_{i=1}^N$ - multi-view dataset**Input:** $\mathcal{G}(\cdot)$ - initialized MVL model**Input:** \mathcal{T} - set of all missing views cases**Output:** $\mathcal{G}(\cdot)$ - Trained MVL model

```

1: for  $(\mathcal{X}^{(i)}, y^{(i)}) \in \mathcal{D}$  do
2:   Obtain  $\mathbf{z}_v^{(i)}$  by forwarding over all view-encoders as Eq. (1)
3:   Initialize  $\mathcal{Y}^{(i)}$  as an empty list
4:   for  $\mathcal{V}^{(j)} \in \mathcal{T}$  do
5:     Obtain  $\mathbf{z}_{F_j}^{(i)}$  from the available views  $\mathcal{V}^{(j)}$  with the dynamic function as Eq. (2)
6:     Obtain  $\hat{y}_j^{(i)}$  by applying  $\mathcal{G}^{head}(\mathbf{z}_{F_j}^{(i)})$ 
7:     Update  $\mathcal{Y}^{(i)}$  by attaching the prediction  $\hat{y}_j^{(i)}$ 
8:   end for
9:   Calculate the loss function based on  $y^{(i)}$  and  $\hat{y}_j^{(i)} \in \mathcal{Y}^{(i)}$  as Eq. (9)
10:  Update  $\mathcal{G}(\cdot)$  by gradient descent
11: end for

```

CropHarvest binary (CropH-b) We use the CropHarvest dataset for crop recognition with four views [Tseng et al., 2021]. This involves a binary task in which the presence of any crop growing at a given location is predicted. It has 69,800 samples around the globe between 2016 and 2021. Each sample has three temporal views: multi-spectral optical (11 bands), radar (2 polarization bands), and weather (2 bands) SITS. These time series have one value per month over 1 year. Besides, the samples have one static view, the topographic information (2 bands). All features have a pixel resolution of 10 m. Furthermore, we use a multi-class version, **CropHarvest multi (CropH-m)**. This is a subset of 29,642 samples with 10 crop types to predict (mutually exclusive), and the same input views from CropH-b.

Live Fuel Moisture Content (LFMC) We use a dataset for moisture content estimation with six views [Rao et al., 2020]. This considers a regression task in which the vegetation water (moisture) per dry biomass (in percentage) in a given location is predicted. There are 2,578 samples in the western US between 2015 and 2019. Each sample has two temporal views: multi-spectral optical (8 bands) and radar (3 bands) SITS. These time series have one value per month over 4 months. In addition, the samples have four static views: topographic information (2 bands), soil properties (3 bands), canopy height (ordinal feature), and land-cover (12 classes). All features were interpolated to a pixel resolution of 250 m.

Particulate Matter 2.5 (PM25) We use a dataset for PM2.5 estimation with three views [Chen, 2017]. This involves a regression task in which the concentration of PM2.5 in the air (in ug/m^3) in a particular city is predicted. The dataset has 167,309 samples in five Chinese cities between 2010 and 2015. Each sample has three temporal views: atmospheric conditions (3 bands), atmospheric dynamics (4 bands), and precipitation (2 bands). The data are at hourly resolution, of which we keep a 3-day window for the estimation, i.e. signals of 72 time-steps are used as input.

4.2 Setup and competing methods

We named our methods using the CoM technique at feature-level as **FCoM-av** (for average), **FCoM-ga** (for gated), **FCoM-cr** (for cross-attention), and **FCoM-me** (for memory fusion). For the cross-attention fusion (FCoM-cr), the function consists of one layer with eight heads and 40% of dropout, while for the memory fusion (FCoM-me), it consists of two bidirectional layers with LSTM units and 40% of dropout. Variations in the selection of these hyperparameters are shown in the A.2.

For comparison, we consider the following supervised methods related to the EO domain. Three methods that perform zero-imputation in the missing views. Two of these use MAug techniques at input-level: **ITempD-co** [Sainte Fare Garnot et al., 2022], using the TempD technique, and **ISensD-co** [Mena et al., 2024b], using the SensD. One method that uses CoM at feature-level: **FCoMI-co** [Gawlikowski et al., 2023], a model that merges by concatenation with a weighted loss and prediction that we extend to multiple views. In addition, we include three methods that ignore the missing views: **FSensD-cr**, adapted from images [Chen et al., 2024] to pixel-wise time series, using cross-attention fusion at feature-level with the SensD technique, **FEmbr-sa** [Choi and Lee, 2019], a feature-level fusion method that randomly samples features from different views in the fused representation, and **ESensI-av**

[Mena et al., 2024b], a view-invariant model using ensemble aggregation (averaging) without MAug techniques. Since self-supervised methods use a bunch of data outside the training set and more input views, we do not consider them because it would not be a fair comparison.

Implementation We apply a z-score normalization to the input data. The categorical and ordinal views (like land-cover and canopy height) are one-hot-vector encoded. We use the best encoder architectures for the selected datasets [Najjar et al., 2024, Mena et al., 2024a]. This corresponds to a 1D CNN encoder for temporal views, and an MLP encoder for static views. We use two layers with 128 units on all encoder architectures, with 20% of dropout and a final layer normalization. After fusion, we use a MLP with one layer as the prediction head. For optimization, we use ADAM optimizer with a batch-size of 128 and early stopping with a patience of five. The stopping criterion is applied over the full-view prediction. The loss function is cross-entropy in classification and mean squared error in regression tasks. We use a weight in the loss function (inverse to the number of samples in each class) to balance the class unbalance in classification. For competing methods, we use 30% of dropout in ITempD-co and the no ratio version in the ISensD-co method [Mena et al., 2024b].

Evaluation We use 10-fold cross-validation repeated three times to reduce results variability. We simulate missing views in the validation fold, as illustrated in Figure 1. We experiment with different degrees of *missingness*: i) moderate missingness, when only one view is missing, ii) extreme missingness, when all views are missing except one. We include the results with no missing views (full-view scenario) for reference. For assessing the predictive performance, we use the F1 Macro (F1) in classification and the Coefficient of Determination (R^2) in regression tasks.

4.3 Results with missing views

In order to assess the effect when a single view is missing, or it is available, we decide to select a few views that individually are the most effective for the task. For this, we train a model individually on each view to predict the task and select the two views that reach the best predictions. We refer to these as the *top* views. For CropH-b, CropH-m, and LFMC these are optical and radar views, as observed in the literature [Hong et al., 2021, Zheng et al., 2021, Mena et al., 2024a], while for PM25 are dynamic and condition views. The results from all the auxiliary views are in the Table 10 in the A.3.

In Table 1 we compare the F1 score of the methods in different cases of missing views for the classification tasks. When there are no missing views or moderate missingness, the best results are obtained by our methods, with FCoM-av and FCoM-ga. However, in extreme cases, our methods become comparable to competing methods. In this extreme missingness, the ESensI-av method effectively handles missing views, competing with our methods and outperforming when only radar view is available. On the other hand, we notice that the methods based on SensD and TempD are highly affected by missing views, i.e. less robust.

For the regression tasks, we display the R^2 in Table 2. Here, the impact of missing views is more severe than in classification, with most methods reaching negative R^2 values in extreme missingness. This difficulty in regression is expected [Mena et al., 2024a] as methods predict a continuous value which disperses in different magnitudes, while in classification the change is only binary, see Sec. 4.5 for a visual illustration. Nonetheless, some of our methods are robust enough and obtain the best results in extreme cases, e.g. FCoM-me. Moreover, our methods (FCoM-av and FCoM-ga) effectively handle the moderate missingness in both datasets. Although the ITempD-co has the best results in the full-view scenario of PM25 data, it has poor robustness, strongly decreasing performance when views

Table 1: Predictive performance in the classification tasks (F1 score) for different cases of missing views (moderate and extreme). The **best** and second best value are highlighted. In parentheses is the number of available views.

Method	CropHarvest binary (CropH-b)					CropHarvest multi (CropH-m)				
	(4/4) No Missing	(3/4) Only missing		(1/4) Only available		(4/4) No Missing	(3/4) Only missing		(1/4) Only available	
	Radar	Optical	Optical	Radar	Radar	Missing	Radar	Optical	Optical	Radar
ITempD-co	0.817 _{±0.008}	0.798 _{±0.009}	0.717 _{±0.013}	0.668 _{±0.015}	0.506 _{±0.075}	0.635 _{±0.017}	0.552 _{±0.019}	0.336 _{±0.021}	0.364 _{±0.029}	0.154 _{±0.017}
ISensD-co	0.787 _{±0.015}	0.780 _{±0.015}	0.747 _{±0.022}	0.765 _{±0.02}	0.572 _{±0.092}	0.608 _{±0.013}	0.587 _{±0.016}	0.437 _{±0.038}	0.587 _{±0.017}	0.207 _{±0.052}
FSensD-cr	0.776 _{±0.045}	0.748 _{±0.091}	0.707 _{±0.106}	0.569 _{±0.21}	0.527 _{±0.169}	0.559 _{±0.126}	0.451 _{±0.232}	0.302 _{±0.173}	0.367 _{±0.259}	0.196 _{±0.169}
FCoMI-co	0.832 _{±0.007}	<u>0.827</u> _{±0.006}	<u>0.804</u> _{±0.006}	0.787 _{±0.010}	0.686 _{±0.010}	0.650 _{±0.020}	0.614 _{±0.019}	0.543 _{±0.014}	0.601 _{±0.019}	0.388 _{±0.015}
FEmbr-sa	0.821 _{±0.007}	0.817 _{±0.007}	0.786 _{±0.007}	0.764 _{±0.008}	0.676 _{±0.012}	0.633 _{±0.015}	0.598 _{±0.022}	0.478 _{±0.015}	0.543 _{±0.024}	0.312 _{±0.012}
ESensI-av	0.802 _{±0.011}	0.806 _{±0.010}	0.767 _{±0.012}	0.791 _{±0.013}	0.701 _{±0.012}	0.605 _{±0.019}	0.577 _{±0.021}	0.478 _{±0.015}	<u>0.635</u> _{±0.023}	0.444 _{±0.022}
FCoM-av	0.837 _{±0.005}	0.834 _{±0.005}	0.804 _{±0.007}	0.809 _{±0.006}	0.615 _{±0.040}	0.686 _{±0.018}	0.648 _{±0.020}	<u>0.549</u> _{±0.011}	0.649 _{±0.018}	0.428 _{±0.017}
FCoM-ga	0.839 _{±0.005}	0.834 _{±0.006}	0.810 _{±0.008}	<u>0.805</u> _{±0.006}	0.681 _{±0.018}	<u>0.678</u> _{±0.016}	<u>0.642</u> _{±0.015}	0.566 _{±0.015}	0.595 _{±0.139}	0.399 _{±0.093}
FCoM-cr	0.826 _{±0.007}	0.823 _{±0.007}	0.799 _{±0.007}	0.801 _{±0.008}	<u>0.693</u> _{±0.008}	0.660 _{±0.019}	0.637 _{±0.019}	<u>0.549</u> _{±0.013}	0.632 _{±0.017}	<u>0.439</u> _{±0.015}
FCoM-me	0.836 _{±0.006}	0.818 _{±0.007}	0.800 _{±0.007}	0.800 _{±0.008}	0.681 _{±0.014}	0.670 _{±0.015}	0.633 _{±0.016}	0.535 _{±0.011}	0.629 _{±0.015}	0.422 _{±0.013}

Table 2: Predictive performance in the regression tasks (R^2 score) for different cases of missing views (moderate and extreme). The **best** and second best values are highlighted. In parentheses is the number of available views. The symbol † represent values below -10.

Method	Live Fuel Moisture Content (LFMC)					Particulate Matter 2.5 (PM25)				
	(6/6) No Missing	(5/6) Only missing Radar	(5/6) Only missing Optical	(1/6) Only available Optical	(1/6) Only available Radar	(3/3) No Missing	(2/3) Only missing Condition	(2/3) Only missing Dynamic	(1/3) Only available Dynamic	(1/3) Only available Condition
ITempD-co	0.691 _{±0.052}	0.036 _{±0.100}	0.036 _{±0.100}	-0.036 _{±0.06}	-0.036 _{±0.06}	0.866 _{±0.093}	0.074 _{±0.035}	-0.124 _{±0.14}	0.073 _{±0.035}	-0.124 _{±0.14}
ISensD-co	0.546 _{±0.053}	0.537 _{±0.047}	0.349 _{±0.053}	0.315 _{±0.057}	0.121 _{±0.049}	0.511 _{±0.058}	0.319 _{±0.065}	0.083 _{±0.056}	0.318 _{±0.066}	0.083 _{±0.056}
FSensD-cr	0.433 _{±0.178}	0.383 _{±0.243}	0.123 _{±0.147}	-0.031 _{±0.557}	-0.264 _{±0.47}	0.187 _{±0.289}	-1.046 _{±2.77}	-0.971 _{±5.10}	-1.091 _{±2.78}	-1.202 _{±5.07}
FCoMI-co	-0.643 _{±2.14}	-0.505 _{±2.17}	-0.434 _{±2.00}	-0.661 _{±2.13}	-1.172 _{±1.93}	-0.316 _{±0.30}	0.157 _{±0.186}	-0.010 _{±0.12}	0.358 _{±0.391}	0.125 _{±0.104}
FEmbr-sa	0.559 _{±0.065}	0.532 _{±0.060}	0.270 _{±0.058}	-5.300 _{±1.80}	-0.796 _{±0.52}	-1.366 _{±4.39}	-0.389 _{±2.51}	-0.135 _{±0.42}	†	-1.077 _{±1.52}
ESensI-av	0.321 _{±0.038}	0.294 _{±0.036}	0.239 _{±0.035}	0.194 _{±0.224}	-0.130 _{±0.36}	0.231 _{±0.077}	0.255 _{±0.059}	0.069 _{±0.106}	0.334 _{±0.078}	0.034 _{±0.135}
FCoM-av	0.628 _{±0.051}	0.606 _{±0.056}	0.435 _{±0.058}	-9.633 _{±12.90}	-7.425 _{±7.24}	0.660 _{±0.103}	0.556 _{±0.162}	-0.441 _{±0.65}	-6.570 _{±3.81}	0.409 _{±0.147}
FCoM-ga	0.700 _{±0.043}	0.683 _{±0.044}	0.491 _{±0.05}	<u>0.326</u> _{±0.09}	<u>0.165</u> _{±0.094}	0.046 _{±0.151}	0.096 _{±0.133}	0.135 _{±0.122}	0.239 _{±0.345}	<u>0.237</u> _{±0.155}
FCoM-cr	0.425 _{±0.154}	0.139 _{±1.187}	0.227 _{±0.153}	-2.403 _{±4.533}	-2.292 _{±3.112}	0.414 _{±0.108}	<u>0.374</u> _{±0.126}	-0.130 _{±0.222}	-0.279 _{±2.271}	-0.203 _{±0.717}
FCoM-me	0.644 _{±0.066}	<u>0.641</u> _{±0.06}	<u>0.479</u> _{±0.061}	0.330 _{±0.072}	0.169 _{±0.077}	-0.033 _{±0.172}	0.079 _{±0.133}	-0.004 _{±0.137}	0.430 _{±0.087}	0.230 _{±0.141}

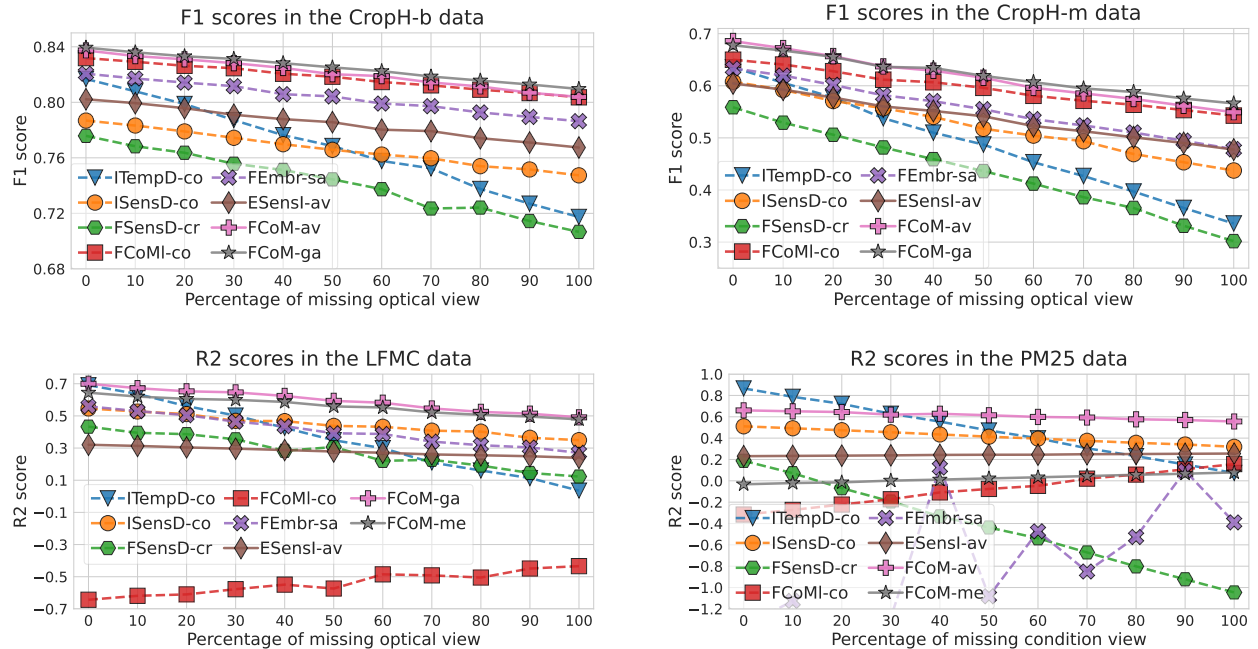


Figure 2: Predictive performance when varying percentages of validation samples have a *top* view missing.

are missing. This outcome is inverse for FCoM-ga, FCoM-me, and FCoMI-co methods, suggesting that these learned missing views scenarios better than full-view ones. Furthermore, leaving the fusion to a random view-selection, as it is the case of FEmbr-sa, does not work in the PM25 data, as it reaches negative R^2 values in all cases.

Overall, we observe that the FCoM-av, despite using the simple aggregation function between the compared ones, performs the best without missing data and in moderate missingness. For the extreme missingness, the best combination for merge function in the CoM depends on the task type. In classification, the best predictions are obtained with FCoM-av and FCoM-cr, while in regression is with FCoM-ga and FCoM-me. Furthermore, some of our methods are greatly affected in these extreme cases. For instance, the FCoM-av method shows a great performance decline in regression. In addition, the baseline FCoMI-co has poor results in most cases of regression, reflecting the poor transferability to other tasks and ineffectiveness of the zero-imputation as observed in the literature [Mena et al., 2024b, Che et al., 2024].

4.4 Results with a fraction of missing views

In Figure 2 we display the predictive performance when one top view for prediction is missing in some samples. We include the results when the other top view is missing in the B.1. We present our two best methods in each dataset.

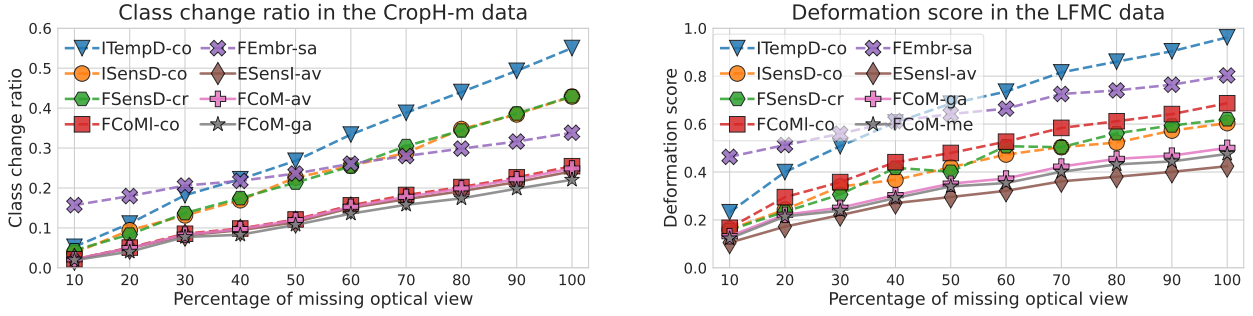


Figure 3: Prediction shift score in classification (class change ratio) and regression (deformation score) tasks.

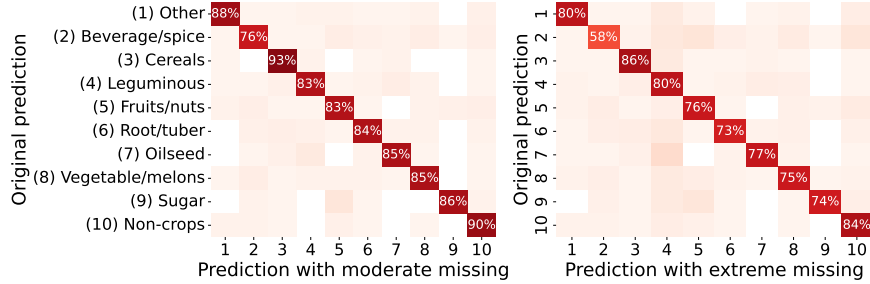


Figure 4: Class prediction shift with moderate (radar view missing), and extreme (optical view available) missingness. The FCoM-ga method is shown in the CropH-m data. The overall class change ratio is 12.5% in the moderate and 20.4% in the extreme cases.

In classification, our FCoM-ga method has the best results along the percentages of missing views, competing with FCoM-av and FCoMI-co. However, the competing method FCoMI-co has a curious behavior in regression, focusing only on the missing views cases and obtaining poor results overall. The FEmbr-sa method also has a strange behavior in the PM25 data, being ineffective for this scenario. In the PM25 data, the ITempD-co method has the best results until 30% of the samples have the condition view missing, from there, the FCoM-av becomes the best. This is due to the greater robustness of our method. Overall, we notice that our methods have the best robustness behavior when the number of samples with missing views increases. This behavior, in the performance curve, corresponds to a good balance between a small slope and a high value.

4.5 Prediction shift due to missing views

We analyze how model predictions are shifted because of missing views, regardless of the target values. We plot the class change ratio and the deformation score at different percentages of missing views in the CropH-m and LPMC data, respectively, in Figure 3. The deformation is calculated as the difference in prediction divided by the deviation of the original prediction, i.e. $RMSE(\hat{y}_{full}, \hat{y}_{miss}) / \text{std}(\hat{y}_{full})$. These graphs show the increase in the prediction shifting when there is more missing data. We observe that the prediction shift curves of our methods are among the three methods with lower values in the comparison, together with FCoMI-co and ESensI-av methods.

As qualitative support for our methods, we plot the class change in the CropH-m data in Figure 4, and the shift in the real-value predicted in the LPMC data in Figure 5. We notice that in moderate missingness, the prediction change in our methods is insignificant, while in extreme cases is shifted to a greater extent. As the predicted value in classification is categorical, the change in prediction is binary (the class change to another one or not), while in the regression task the predicting value is continuous. Therefore, we can see how the prediction is dispersed from the original value to different degrees for all samples.

4.6 Execution time comparison

We compare the execution time of different methods in Figure 6. During training, we observe that the methods ignoring missing views lead to the most efficient training time, i.e. FSensD-cr, ESensI-av, and FCoM-av. However, we notice that the combination of the CoM technique with sophisticated merge functions (-ga, -cr, and -me suffix)

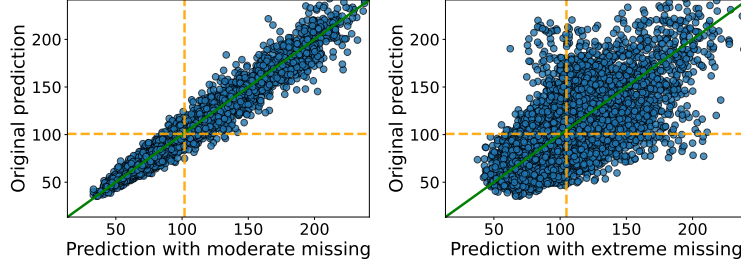


Figure 5: Real-value prediction shift with moderate (radar view missing), and extreme (only optical view available). The FCoM-ga method is shown in the LFMC data. The overall deformation score is 0.208 in moderate and 0.722 in extreme cases.

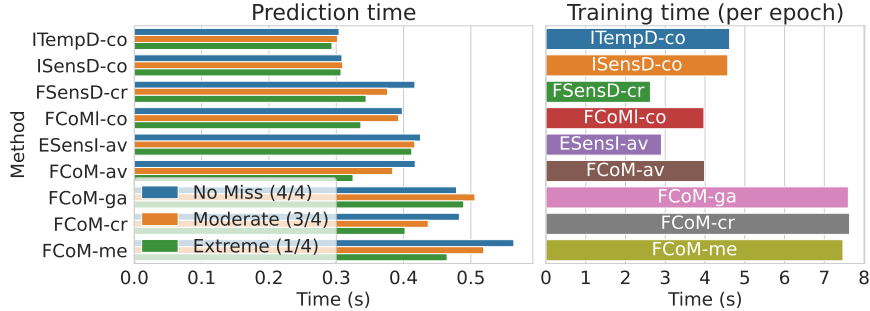


Figure 6: Execution time of different MVL methods. The times are calculated in the CropH-m data with 4 views. Prediction times are separated into no missing (4/4), only one view missing (3/4) and only one view available (1/4).

increases training time (per epoch) by almost double. On the other side, the most efficient prediction time over the entire dataset is associated with the models using input-level fusion. This is expected as these methods use a single encoder architecture. Nevertheless, we notice that our methods have a more efficient execution time when there is more missing data, i.e. by ignoring missing views the model dynamical adapts to perform calculations on just the available data (no fake data insertion).

5 Analysis and limitation

We show the effect of applying MAugs at different levels of the MVL models with average fusion in Table 3. Similar results are obtained with other merge functions (see B.2). We zero-impute views if they are missing at input-level, and ignore them if missing at feature-level. We notice a trend to increase the model robustness to missing views when the CoM is used, compared to SensD and without MAugs. Randomly dropping sensors, used in [Chen et al., 2024, Mena et al., 2024b], have good relative robustness but quite low overall performance. In the LFMC data, we find it more effective to address missing views at the input rather than feature level, as noted in the literature [Mena et al., 2024a]. However, with the CoM technique, we notice that is better to use it at feature by ignoring than at input-level with zero imputation. Besides, the CoM even allows increasing the full-view performance in the CropH-m data. The evidence suggests that, in most cases, our usage of CoM at feature-level and dynamic fusion is optimal for model robustness.

Along the results, we note a slight variation in which method obtains the best results for each dataset and missing view scenario. However, this variability is expected in the EO field, as the data is quite heterogeneous and region-dependent [Camps-Valls et al., 2021, Hong et al., 2021, Ofori-Ampofo et al., 2021, Mena et al., 2023, Rolf et al., 2024]. In addition, this variation depends on the metrics used to assess the models. In our study, standard performance metrics are used from the literature. However, additional values are included in the C. Nevertheless, our combination of CoM with the simple average function (FCoM-av) shows good overall results, without significantly increasing the training time, as well as having an adaptive prediction time based on the available views.

We remark that Transformer models are not naturally robust to missing data [Ma et al., 2022]. They can handle missing data without intervention, but that does not imply they will obtain the same performance as when there is no missing

Table 3: Different MAug techniques applied at input (concatenation) and feature (average) level. The † is a value below -10.

		Croph-m (F1 scores)					LFMC (R^2 scores)				
MAug	Level	(4/4) No Missing	(3/4) Only missing Radar	(3/4) Only missing Optical	(1/4) Only available Optical	(1/4) Only available Radar	(6/6) No Missing	(5/6) Only missing Radar	(5/6) Only missing Optical	(1/6) Only available Optical	(1/6) Only available Radar
-	Input	0.655	0.569	0.359	0.230	0.081	0.638	0.593	0.262	0.293	0.057
SensD	Input	0.566	0.522	0.422	0.401	0.206	0.506	0.468	0.342	0.305	0.134
CoM	Input	0.652	0.637	0.385	0.602	0.123	0.515	0.484	0.355	0.317	0.118
-	Feature	0.647	0.561	0.492	0.269	0.224	0.648	0.531	0.151	†	†
SensD	Feature	0.634	0.615	0.526	0.590	0.386	0.511	0.496	0.302	†	-1.709
CoM	Feature	0.679	0.646	0.549	0.645	0.430	0.625	0.604	0.437	-9.632	-8.362

data [Du et al., 2023, Chen et al., 2024]. For instance, in our case, we show that by using the cross-attention fusion (based on Transformer models) is not optimal for our problem.

Regarding the limitations, we state that the CoM technique is dependent on the total views of each dataset (m), since the number of augmented samples in the CoM technique depends on this: $2^m - 1$. In addition, we assess the effect of missing views only at inference, assuming a full-view training dataset. However, based on the dynamic fusion, it could be easily extended to other settings. Furthermore, we validate our methods using pixel-wise EO datasets. Although this validation is conducted across four datasets, its effectiveness in other domains needs to be verified.

6 Conclusion

We introduce Missing data as Augmentation (MAug) technique tailored to Multi-View Learning (MVL) with missing views, named Combinations of Missing views (CoM). We apply this technique at feature-level in combination with dynamic merge functions. For evaluation, we simulate missing views during inference to assess model robustness (predictive performance decay) in two scenarios. Moderate missingness, when only *top* views (the ones with the best individual performance) are missing, and extreme missingness, when only one *top* view is available. Our findings show that our approaches outperform competing methods in moderate missingness, particularly with FCoM-av. Moreover, due to the MAug effect, we see an increase in the classification performance in the full-view scenario. In addition, we identify challenging scenarios for robustness, particularly in regression tasks and extreme missingness. For these challenges, future work should consider developing models that operate with any available data at decision-level fusion, such as by weighing predictions with missing data.

Acknowledgments

F. Mena acknowledge support through a scholarship of the University of Kaiserslautern-Landau.

Data and code availability

The data used in this manuscript corresponds to public benchmark datasets released in [Tseng et al., 2021, Rao et al., 2020, Chen, 2017]. We provide functions to facilitate the processing of these to a machine learning ready structure. This is available on our GitHub at <https://github.com/fmenat/com-views>.

References

- [Astruc et al., 2025] Astruc, G., Gonthier, N., Mallet, C., and Landrieu, L. (2025). Omnisat: Self-supervised modality fusion for earth observation. In *European Conference on Computer Vision*, pages 409–427. Springer.
- [Audebert et al., 2018] Audebert, N., Le Saux, B., and Lefèvre, S. (2018). Beyond RGB: Very high resolution urban remote sensing with multimodal deep networks. *ISPRS Journal of Photogrammetry and Remote Sensing*, 140:20–32.
- [Bouthillier et al., 2015] Bouthillier, X., Konda, K., Vincent, P., and Memisevic, R. (2015). Dropout as data augmentation. *arXiv preprint arXiv:1506.08700*.
- [Bugeño and Mendoza, 2020] Bugeño, M. and Mendoza, M. (2020). Learning to combine classifiers outputs with the Transformer for text classification. *Intelligent Data Analysis*, 24(S1):15–41.

- [Camps-Valls et al., 2021] Camps-Valls, G., Tuia, D., Zhu, X. X., and Reichstein, M. (2021). *Deep learning for the Earth Sciences: A comprehensive approach to remote sensing, climate science and geosciences*. John Wiley & Sons, New York.
- [Cao et al., 2018] Cao, W., Wang, D., Li, J., Zhou, H., Li, L., and Li, Y. (2018). BRITS: Bidirectional recurrent imputation for time series. *Advances in Neural Information Processing Systems (NIPS)*, 31.
- [Che et al., 2024] Che, X., Zhang, H. K., Li, Z. B., Wang, Y., Sun, Q., Luo, D., and Wang, H. (2024). Linearly interpolating missing values in time series helps little for land cover classification using recurrent or attention networks. *ISPRS Journal of Photogrammetry and Remote Sensing*, 212:73–95.
- [Chen, 2017] Chen, S. (2017). PM2.5 Data of Five Chinese Cities. UCI Machine Learning Repository.
- [Chen et al., 2024] Chen, Y., Zhao, M., and Bruzzone, L. (2024). A novel approach to incomplete multimodal learning for remote sensing data fusion. *IEEE Transactions on Geoscience and Remote Sensing*.
- [Choi and Lee, 2019] Choi, J.-H. and Lee, J.-S. (2019). EmbraceNet: A robust deep learning architecture for multimodal classification. *Information Fusion*, 51:259–270.
- [Cong et al., 2022] Cong, Y., Khanna, S., Meng, C., Liu, P., Rozi, E., He, Y., Burke, M., Lobell, D., and Ermon, S. (2022). Satmae: Pre-training transformers for temporal and multi-spectral satellite imagery. *Advances in Neural Information Processing Systems*, 35:197–211.
- [Devlin et al., 2018] Devlin, J., Chang, M.-W., Lee, K., and Toutanova, K. (2018). BERT: Pre-training of deep bidirectional transformers for language understanding. In *Proceedings of the Conference of the North American Chapter of the Association for Computational Linguistics: Human Language Technologies (NAACL-HLT)*, pages 4171–4186.
- [Du et al., 2023] Du, W., Côté, D., and Liu, Y. (2023). SAITS: Self-attention-based imputation for time series. *Expert Systems with Applications*, 219:119619.
- [Ebel et al., 2023] Ebel, P., Garnot, V. S. F., Schmitt, M., Wegner, J. D., and Zhu, X. X. (2023). UnCRtainTS: Uncertainty quantification for cloud removal in optical satellite time series. In *Proceedings of the IEEE/CVF Conference on Computer Vision and Pattern Recognition (CVPR)*, pages 2085–2095.
- [Ekim and Schmitt, 2024] Ekim, B. and Schmitt, M. (2024). Deep occlusion framework for multimodal earth observation data. *IEEE Geoscience and Remote Sensing Letters*.
- [Fasnacht et al., 2020] Fasnacht, L., Renard, P., and Brunner, P. (2020). Robust input layer for neural networks for hyperspectral classification of data with missing bands. *Applied Computing and Geosciences*, 8:100034.
- [Ferrari et al., 2023] Ferrari, F., Ferreira, M. P., Almeida, C. A., and Feitosa, R. Q. (2023). Fusing Sentinel-1 and Sentinel-2 images for deforestation detection in the Brazilian Amazon under diverse cloud conditions. *IEEE Geoscience and Remote Sensing Letters*, 20:1–5.
- [Francis, 2024] Francis, A. (2024). Sensor independent cloud and shadow masking with partial labels and multimodal inputs. *IEEE Transactions on Geoscience and Remote Sensing*.
- [Gawlikowski et al., 2023] Gawlikowski, J., Saha, S., Niebling, J., and Zhu, X. X. (2023). Handling unexpected inputs: Incorporating source-wise out-of-distribution detection into SAR-optical data fusion for scene classification. *EURASIP Journal on Advances in Signal Processing*, 2023(1):47.
- [Ghamisi et al., 2016] Ghamisi, P., Höfle, B., and Zhu, X. X. (2016). Hyperspectral and LiDAR data fusion using extinction profiles and deep convolutional neural network. *IEEE Journal of Selected Topics in Applied Earth Observations and Remote Sensing*, 10(6):3011–3024.
- [Guo et al., 2024] Guo, X., Lao, J., Dang, B., Zhang, Y., Yu, L., Ru, L., Zhong, L., Huang, Z., Wu, K., Hu, D., et al. (2024). Skysense: A multi-modal remote sensing foundation model towards universal interpretation for Earth observation imagery. In *Proceedings of the IEEE/CVF Conference on Computer Vision and Pattern Recognition*, pages 27672–27683.
- [Haut et al., 2019] Haut, J. M., Paoletti, M. E., Plaza, J., Plaza, A., and Li, J. (2019). Hyperspectral image classification using random occlusion data augmentation. *IEEE Geoscience and Remote Sensing Letters*, 16(11):1751–1755.
- [He et al., 2022] He, K., Chen, X., Xie, S., Li, Y., Dollár, P., and Girshick, R. (2022). Masked autoencoders are scalable vision learners. In *Proceedings of the IEEE/CVF Conference on Computer Vision and Pattern Recognition (CVPR)*, pages 16000–16009.
- [Heinrich et al., 2023] Heinrich, R., Scholz, C., Vogt, S., and Lehna, M. (2023). Targeted adversarial attacks on wind power forecasts. *Machine Learning*.
- [Hong et al., 2021] Hong, D., Gao, L., Yokoya, N., Yao, J., Chanussot, J., Du, Q., and Zhang, B. (2021). More diverse means better: Multimodal deep learning meets remote-sensing imagery classification. *IEEE Transactions on Geoscience and Remote Sensing*, 59(5):4340–4354.

- [Inglada et al., 2016] Inglada, J., Vincent, A., Arias, M., and Marais-Sicre, C. (2016). Improved early crop type identification by joint use of high temporal resolution SAR and optical image time series. *Remote Sensing*, 8(5):362.
- [Kussul et al., 2017] Kussul, N., Lavreniuk, M., Skakun, S., and Shelestov, A. (2017). Deep learning classification of land cover and crop types using remote sensing data. *IEEE Geoscience and Remote Sensing Letters*, 14(5):778–782.
- [Lee et al., 2019] Lee, J., Lee, Y., Kim, J., Kosiorek, A., Choi, S., and Teh, Y. W. (2019). Set Transformer: A framework for attention-based permutation-invariant neural networks. In *International Conference on Machine Learning (ICML)*, pages 3744–3753. PMLR.
- [Ma et al., 2022] Ma, M., Ren, J., Zhao, L., Testuggine, D., and Peng, X. (2022). Are multimodal transformers robust to missing modality? In *Proceedings of the IEEE/CVF Conference on Computer Vision and Pattern Recognition (CVPR)*, pages 18177–18186.
- [Mena et al., 2024a] Mena, F., Arenas, D., Charfuelan, M., Nuske, M., and Dengel, A. (2024a). Impact assessment of missing data in model predictions for earth observation applications. In *Proceedings of the IEEE International Geoscience and Remote Sensing Symposium (IGARSS)*, pages 967–971.
- [Mena et al., 2024b] Mena, F., Arenas, D., and Dengel, A. (2024b). Increasing the robustness of model predictions to missing sensors in earth observation. *arXiv preprint arXiv:2407.15512*.
- [Mena et al., 2023] Mena, F., Arenas, D., Nuske, M., and Dengel, A. (2023). A comparative assessment of multi-view fusion learning for crop classification. In *Proceedings of the IEEE International Geoscience and Remote Sensing Symposium (IGARSS)*, pages 5631–5634. IEEE.
- [Mena et al., 2024c] Mena, F., Arenas, D., Nuske, M., and Dengel, A. (2024c). Common practices and taxonomy in deep multi-view fusion for remote sensing applications. *IEEE Journal of Selected Topics in Applied Earth Observations and Remote Sensing*, pages 4797 – 4818.
- [Mena et al., 2024d] Mena, F., Pathak, D., Najjar, H., Sanchez, C., Helber, P., Bischke, B., Habelitz, P., Miranda, M., Siddamsetty, J., Nuske, M., et al. (2024d). Adaptive fusion of multi-view remote sensing data for optimal sub-field crop yield prediction. *arXiv preprint arXiv:2401.11844*.
- [Najjar et al., 2024] Najjar, H., Nuske, M., and Dengel, A. (2024). Data-centric machine learning for earth observation: Necessary and sufficient features. *arXiv preprint arXiv:2408.11384*.
- [Ofori-Ampofo et al., 2021] Ofori-Ampofo, S., Pelletier, C., and Lang, S. (2021). Crop type mapping from optical and radar time series using attention-based deep learning. *Remote Sensing*, 13(22).
- [Rao et al., 2020] Rao, K., Williams, A. P., Flefil, J. F., and Konings, A. G. (2020). SAR-enhanced mapping of live fuel moisture content. *Remote Sensing of Environment*, 245:111797.
- [Rolf et al., 2024] Rolf, E., Klemmer, K., Robinson, C., and Kerner, H. (2024). Mission critical–Satellite data is a distinct modality in machine learning. *arXiv preprint arXiv:2402.01444*.
- [Sainte Fare Garnot et al., 2022] Sainte Fare Garnot, V., Landrieu, L., and Chehata, N. (2022). Multi-modal temporal attention models for crop mapping from satellite time series. *ISPRS Journal of Photogrammetry and Remote Sensing*, 187:294–305.
- [Shen et al., 2015] Shen, H., Li, X., Cheng, Q., Zeng, C., Yang, G., Li, H., and Zhang, L. (2015). Missing information reconstruction of remote sensing data: A technical review. *IEEE Geoscience and Remote Sensing Magazine*, 3(3):61–85.
- [Srivastava et al., 2014] Srivastava, N., Hinton, G., Krizhevsky, A., Sutskever, I., and Salakhutdinov, R. (2014). Dropout: a simple way to prevent neural networks from overfitting. *Journal of Machine Learning Research*, 15(1):1929–1958.
- [Tseng et al., 2021] Tseng, G., Zvonkov, I., Nakalembe, C. L., and Kerner, H. (2021). CropHarvest: A global dataset for crop-type classification. *Proceedings of NIPS Datasets and Benchmarks Track*.
- [Tseng et al., 2023] Tseng, G., Zvonkov, I., Purohit, M., Rolnick, D., and Kerner, H. (2023). Lightweight, pre-trained transformers for remote sensing timeseries. *arXiv preprint arXiv:2304.14065*.
- [Vaswani et al., 2017] Vaswani, A., Shazeer, N., Parmar, N., Uszkoreit, J., Jones, L., Gomez, A. N., Kaiser, Ł., and Polosukhin, I. (2017). Attention is all you need. *Advances in Neural Information Processing Systems (NIPS)*, 30.
- [Wang et al., 2021] Wang, C., Liu, X., Pei, J., Huang, Y., Zhang, Y., and Yang, J. (2021). Multiview attention CNN-LSTM network for SAR automatic target recognition. *IEEE Journal of Selected Topics in Applied Earth Observations and Remote Sensing*, 14:12504–12513.
- [Wang et al., 2022] Wang, Y., Albrecht, C. M., and Zhu, X. X. (2022). Self-supervised vision transformers for joint SAR-optical representation learning. In *Proceedings of the IEEE International Geoscience and Remote Sensing Symposium (IGARSS)*, pages 139–142.

- [Yan et al., 2021] Yan, X., Hu, S., Mao, Y., Ye, Y., and Yu, H. (2021). Deep multi-view learning methods: A review. *Neurocomputing*, 448:106–129.
- [Yuan et al., 2022] Yuan, Y., Lin, L., Liu, Q., Hang, R., and Zhou, Z.-G. (2022). SITS-Former: A pre-trained spatio-spectral-temporal representation model for Sentinel-2 time series classification. *International Journal of Applied Earth Observation and Geoinformation*, 106:102651.
- [Zhang et al., 2020] Zhang, P., Du, P., Lin, C., Wang, X., Li, E., Xue, Z., and Bai, X. (2020). A hybrid attention-aware fusion network (HAFNet) for building extraction from high-resolution imagery and LiDAR data. *Remote Sensing*, 12(22).
- [Zheng et al., 2021] Zheng, Z., Ma, A., Zhang, L., and Zhong, Y. (2021). Deep multisensor learning for missing-modality all-weather mapping. *ISPRS Journal of Photogrammetry and Remote Sensing*, 174:254–264.

A Initial setup

A.1 Dataset Description

We show the features from each view in the different datasets in Tables 4, 5, and 6 for PM25, CropHarvest, and LFMC data respectively. The abbreviations used in the tables correspond to: normalized difference vegetation index (NDVI), normalized difference water index (NDWI), and near infrared vegetation index (NIRv).

Table 4: Name of features in each view in the **PM25** data [Chen, 2017]. The source of the views are ground-based stations.

View	Features
Conditions	dew point, temperature, and humidity
Dynamics	pressure, combined wind direction, cumulated wind speed, season
Precipitation	precipitation, and cumulated precipitation

Table 5: Name of features in each view in the **CropH-b** and **CropH-m** data [Tseng et al., 2021]. The views are at 10 m spatial resolution.

View	Source	Features
Optical	Sentinel-2 (level 1C)	B2 (blue), B3 (green), B4 (red), B5, B6, B7, B8, B8A, B9, B11, B12, NDVI
Radar	Sentinel-1 (C-band)	VV and VH polarization bands
Weather	ERA5	temperature and precipitation
Topographic	NASA’s SRTM	elevation and slope

Table 6: Name of features in each view in the **LFMC** data [Rao et al., 2020]. The views are at 250 m spatial resolution.

View	Source	Features
Optical	Landsat 8	red, green, blue, near infrared, short-wave infrared, NDVI, NDWI, NIRv
Radar	Sentinel-1 (C-Band)	VV, VH, and VH/VV polarization bands
Topographic	National Elevation Database	elevation and slope
Soil	Unified North American Soil Map	silt, sand, and clay
LiDAR	Global Laser Altimetry System	canopy height (ordinal value)
Land-cover	GLOBCOVER	class label between 12 options

A.2 Architecture Selection

In Table 7 we compare the MAug techniques to a view-permutation in the memory-based fusion with a LSTM architecture. Since views are processed sequentially, the view-permutation is included to prevent the model from overfitting the views order [Lee et al., 2019]. We observe that the usage of the MAug technique has a greater positive effect on the predictive performance than the view-permutation in the full-view scenario and with missing views. This suggests that the memory fusion with the MAug does not require an explicit permutation to become order invariant and increase generalization. Nevertheless, the good behavior without permutation in LFMC data might be just overfitting, caused by the small dataset (less than 2000 samples to train).

In Table 8 we compare different architectures of the memory fusion. We notice a tendency to get better results (in full-view and with missing views) with a more complex network architecture. Overall, the best results are obtained with two bidirectional LSTM layers, while the second best results are associated with an architecture based on GRU layers.

In Table 9 we compare different architectural options of the cross-attention fusion, based on Transformer layers. We observe an optimal value across datasets and missing scenarios with eight heads and just one layer. Besides, we notice a slight tendency to get better results when using a more complex network architecture.

Table 7: Memory fusion-based MVL model with different configurations of view-permutation and MAug techniques.

MAug	Permutation	CropH-m (F1)		LFMC (R^2)	
		No Missing	Missing Optical	No Missing	Missing Optical
-	-	0.656	0.503	0.735	0.095
-	All	0.649	0.487	<u>0.706</u>	0.192
SensD	All	0.643	0.536	0.551	0.353
-	Random	0.643	0.496	0.666	0.224
SensD	Random	0.641	0.531	0.507	0.327
CoM	Random	<u>0.666</u>	<u>0.555</u>	0.595	<u>0.428</u>
CoM	-	0.672	0.559	0.613	0.412

Table 8: Memory fusion-based MVL model with different network architectures. ‘‘Bi’’ stands for bidirectional layer.

Gate	Layers	CropH-m (F1)		LFMC (R^2)	
		No Missing	Missing Optical	No Missing	Missing Optical
GRU	1	0.666	<u>0.554</u>	0.627	0.422
GRU	1 (Bi)	<u>0.671</u>	<u>0.554</u>	<u>0.636</u>	0.451
GRU	2 (Bi)	0.663	0.552	0.634	<u>0.468</u>
GRU	3 (Bi)	0.661	0.546	0.626	<u>0.450</u>
LSTM	1 (Bi)	0.670	0.552	0.634	0.461
LSTM	2 (Bi)	0.677	0.557	0.657	0.477

Table 9: Cross-attention fusion-based MVL model with different network architectures.

Heads	Layers	CropH-m (F1)		LFMC (R^2)	
		No missing	Missing optical	No missing	Missing optical
1	1	0.637	0.468	0.545	0.375
2	1	0.622	0.462	0.551	<u>0.380</u>
4	1	0.650	0.511	<u>0.553</u>	<u>0.380</u>
4	2	<u>0.654</u>	0.511	0.536	0.351
8	1	0.659	0.520	0.569	0.400
8	2	0.650	0.504	0.541	0.371
8	3	0.652	<u>0.519</u>	0.541	0.362

A.3 Individual view performance

In order to detect the *top* views for prediction in each dataset, we train an individual model on each view. The results for each dataset are shown in Table 10. For CropH-b, CropH-m, and LFMC these are optical and radar views, while for the PM25 dataset the top views are dynamic and condition. We note that the static views usually have a low predictive performance, only serving as a complement to the *top* views for prediction.

Table 10: Predictive performance of individually trained models (per view). The F1 scores are shown in classification tasks and R^2 scores in the regression tasks. The **best** and second best values are highlighted.

View	CropH-b	CropH-m	LFMC	PM25
Optical	0.791 _{-0.013}	0.635 _{-0.023}	0.194 _{-0.224}	
Radar	<u>0.752</u> _{-0.012}	<u>0.444</u> _{-0.022}	<u>0.050</u> _{-0.360}	
Topographic	0.631 _{-0.044}	0.095 _{-0.028}	-0.124 _{-0.590}	
Weather	0.701 _{-0.012}	0.346 _{-0.013}		
Soil			-0.245 _{-0.557}	
LiDAR			-0.033 _{-0.147}	
Land-cover			-0.021 _{-0.102}	
Conditions				<u>0.034</u> _{-0.135}
Dynamics				0.334 _{-0.078}
Precipitation				-0.072 _{-0.068}

B Additional results

B.1 Another top view missing

In Figure 7 we display the predictive performance in all datasets when additional views are missing in some samples, as a complement to Figure 2. We present our two best methods in each dataset. In the classification tasks, the proposed FCoM-ga method has the best predictive performance along the percentage of missing data, as observed when the top view is missing (Figure 2). Overall, our methods show the best behavior (of a good balance between a small slope and a high value) when increasing the level of samples with missing views. Furthermore, most of the methods have a high robustness to missing the radar view in the classification tasks. Surprisingly, FCoM-av has a strange behavior in the PM25 data, being the only one greatly affected by missing the precipitation view. Perhaps our method learned a prediction quite dependent on this view in that dataset.

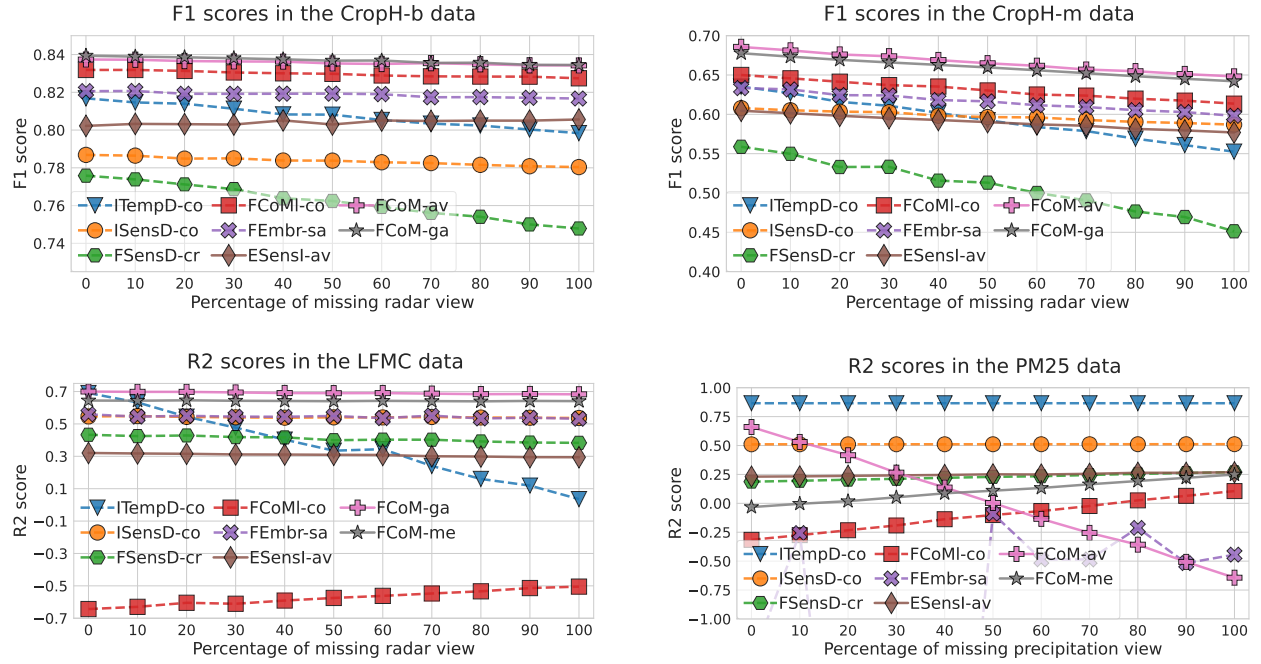


Figure 7: Predictive performance and robustness when varying percentages of validation samples have a *top* view missing.

B.2 Dynamic merge function comparison

We analyze the effect of applying two MAug techniques at different levels of the MVL models, similar to Table 3 that shows this analysis for average fusion. The Table 11, Tables 12, and Tables 13 include the results when using gated fusion, cross-attention fusion, and memory fusion respectively. When views are missing at input-level, they are imputed, and when views are missing at feature-level, they are ignored. We notice the same behavior observed for the

Table 11: Different configurations of the MAug technique applied at input or feature level with **gated fusion**. The F1 scores are shown in the CropH-m data and R^2 scores in the LFCM data. The † is a value below -10.

		CropH-m (F1)					LFCM (R^2)				
MAug	Level	(4/4) No missing	Only missing (3/4)		Only available (1/4)		(6/6) No missing	Only missing (5/6)		Only available (1/6)	
			Radar	Optical	Optical	Radar		Radar	Optical	Optical	Radar
-	Input	0.643	0.506	0.354	0.189	0.073	<u>0.735</u>	0.631	0.238	0.215	-0.011
SensD	Input	0.592	0.562	0.479	0.505	0.323	0.545	0.522	0.324	-3.148	-5.625
CoM	Input	0.662	0.619	0.417	0.565	0.089	0.615	0.620	0.292	<u>0.234</u>	<u>0.012</u>
-	Feature	0.653	0.574	0.494	0.355	0.250	0.738	<u>0.660</u>	0.225	†	†
SensD	Feature	0.668	0.632	0.538	0.610	0.387	0.532	0.499	0.336	-3.151	-0.550
CoM	Feature	0.678	0.647	0.568	0.627	0.418	0.684	0.678	0.471	0.326	0.158

Table 12: Different configurations of the MAug technique applied at input or feature level with **cross-attention fusion**. The F1 scores are shown in the CropH-m data and R^2 scores in the LFMC data. The † is a value below -10.

		CropH-m (F1)					LFMC (R^2)				
MAug	Level	(4/4) No missing	Only missing (3/4)		Only available (1/4)		(6/6) No missing	Only missing (5/6)		Only available (1/6)	
			Radar	Optical	Optical	Radar		Radar	Optical	Optical	Radar
-	Input	0.646	0.585	0.239	0.432	0.072	<u>0.575</u>	0.521	0.289	<u>0.242</u>	<u>0.053</u>
SensD	Input	0.569	0.54	0.438	0.523	0.302	0.522	0.503	0.303	-0.005	-0.205
CoM	Input	<u>0.655</u>	0.636	0.216	0.620	0.071	0.554	0.481	0.361	0.295	0.089
-	Feature	0.637	0.589	0.495	0.506	0.287	0.579	0.539	-0.388	-0.058	-2.702
SensD	Feature	0.639	<u>0.616</u>	<u>0.510</u>	<u>0.617</u>	<u>0.403</u>	0.536	<u>0.525</u>	<u>0.315</u>	0.013	0.019
CoM	Feature	0.665	0.636	0.547	0.638	0.441	0.520	0.471	0.278	-0.363	-1.005

Table 13: Different configurations of the MAug technique applied at input or feature level with **memory fusion**. The F1 scores are shown in the CropH-m data and R^2 scores are shown in the LFMC data.

		CropH-m (F1)					LFMC (R^2)				
MAug	Level	(4/4) No missing	Only missing (3/4)		Only available (1/4)		(6/6) No missing	Only missing (5/6)		Only available (1/6)	
			Radar	Optical	Optical	Radar		Radar	Optical	Optical	Radar
-	Input	0.651	0.572	0.492	0.287	0.237	<u>0.735</u>	<u>0.634</u>	0.072	-4.165	†
SensD	Input	0.586	0.547	0.471	0.490	0.319	0.568	0.549	0.359	-0.015	-0.383
CoM	Input	0.662	0.630	<u>0.556</u>	0.618	0.413	0.648	0.630	0.420	0.346	<u>0.146</u>
-	Feature	0.641	0.568	0.499	0.316	0.235	0.741	0.671	0.022	-0.753	-3.337
SensD	Feature	0.638	0.610	0.533	0.594	0.378	0.557	0.547	0.372	-0.410	-0.045
CoM	Feature	<u>0.661</u>	<u>0.624</u>	0.558	<u>0.617</u>	0.421	0.548	0.563	<u>0.410</u>	<u>0.342</u>	0.155

average, i.e. i) tendency to increase the model robustness to missing data when the CoM technique is used, compared to SensD and without MAug techniques, ii) generalization behavior (increase in performance) of MAug techniques when there is no missing views. Nevertheless, we notice that in some cases the MAug technique impairs the model performance due to the difficulty in estimating the target with missing views.

C Results with additional metrics

We assess the predictive performance with alternative metrics: area under the curve (AUC) of the precision-recall plot in classification, and mean average percentage error (MAPE) in regression tasks. In addition, for assessing the robustness, we use the Performance Robustness Score (PRS) presented in [Heinrich et al., 2023]. The PRS is based on the predictive error with missing views relative to the predictive error in the full-view scenario:

$$\text{PRS}(y, \hat{y}_{\text{miss}}, \hat{y}_{\text{full}}) = \exp\left(1 - \frac{\text{RMSE}(y, \hat{y}_{\text{miss}})}{\text{RMSE}(y, \hat{y}_{\text{full}})}\right), \quad (10)$$

then it is normalized as $\text{PRS} = \min(1, \text{PRS})$. The results for the CropH-b, CropH-m, LFMC, and PM25 data are in Tables 14, 15, 16, and 17 respectively. We notice that the model robustness cannot be assessed only with relative robustness metrics, such as PRS. This is because the relative metrics hide the overall predictive performance. For instance, a horizontal line behavior in Figure 2, such as from ISensD-co, will get a PRS of one, independently of the position of this line on the y-axis (performance). Even, in some cases, the prediction shift due to missing views can go towards correcting the original prediction, as shown in FCoMI-co in Figure 2. In our work, we include these metrics for further analysis, but metrics that can mix these concepts could allow a more succinct analysis.

We plot the PRS value when different number of samples have the top views missing in Figure 8. We notice a different behavior in this relative score compared to results in Figure 2. In the PRS analysis, the best results are obtained by the ESensI-av method followed by FCoMI-co. The curve of our methods are between the third and fourth best position in this relative score. This reflects that, despite the good behavior of our methods in the predictive performance, there is still a gap in reaching the predictive robustness (based on PRS) of the competing methods, such as the one of ESensI-av.

Table 14: Additional results for different cases of missing views (moderate and extreme) in the **CropH-b** data. We highlight the **best** and **second best** value in each scenario. The value in parentheses is the number of available views.

Method	AUC value (\uparrow)					PRS value (\uparrow)			
	(4/4) No Missing	(3/4) Only missing		(1/4) Only available		(3/4) Only missing		(1/4) Only available	
		Radar	Optical	Optical	Radar	Radar	Optical	Optical	Radar
ITempD-co	0.920	0.908	0.813	0.772	0.666	0.958	0.810	0.761	0.606
ISensD-co	0.903	0.899	0.864	0.869	0.736	0.984	0.930	<u>0.982</u>	<u>0.739</u>
FSensD-cr	0.876	0.847	0.798	0.687	0.637	0.950	0.861	0.783	0.665
FCoMI-co	0.930	<u>0.925</u>	0.903	0.889	0.791	0.996	0.948	0.906	0.733
FEmbr-sa	0.923	0.917	0.889	0.866	0.763	0.987	0.915	0.800	0.651
ESensI-av	0.907	0.907	0.879	0.900	0.805	0.996	<u>0.943</u>	0.995	0.863
FCoM-av	<u>0.933</u>	0.931	<u>0.912</u>	0.908	0.800	<u>0.991</u>	0.890	0.859	0.478
FCoM-ga	0.934	0.931	0.915	<u>0.904</u>	<u>0.801</u>	0.986	0.908	0.897	0.645
FCoM-cr	0.925	0.922	0.903	0.901	0.800	0.991	0.922	0.919	0.672
FCoM-me	0.932	0.921	0.908	0.903	0.800	0.944	0.899	0.904	0.682

Table 15: Additional results for different cases of missing views (moderate and extreme) in the **CropH-m** data. We highlight the **best** and **second best** value in each scenario. The value in parentheses is the number of available views.

Method	AUC value (\uparrow)					PRS value (\uparrow)			
	(4/4) No Missing	(3/4) Only missing		(1/4) Only available		(3/4) Only missing		(1/4) Only available	
		Radar	Optical	Optical	Radar	Radar	Optical	Optical	Radar
ITempD-co	0.962	0.946	0.837	0.850	0.661	0.893	0.674	0.716	0.649
ISensD-co	0.904	0.869	0.732	0.760	0.595	0.937	0.759	0.821	0.718
FSensD-cr	0.928	0.864	0.796	0.779	0.673	0.905	0.769	0.834	0.695
FCoMI-co	0.964	0.958	<u>0.937</u>	0.945	0.856	<u>0.953</u>	<u>0.894</u>	<u>0.950</u>	<u>0.776</u>
FEmbr-sa	0.956	0.950	0.911	0.929	0.797	0.937	0.820	0.761	0.562
ESensI-av	0.948	0.945	0.912	0.957	0.885	0.971	0.895	0.991	0.884
FCoM-av	0.967	0.962	<u>0.937</u>	<u>0.954</u>	0.864	0.929	0.810	0.851	0.622
FCoM-ga	0.967	0.962	0.944	0.932	0.854	0.938	0.838	0.885	0.661
FCoM-cr	0.962	0.958	0.935	0.953	<u>0.875</u>	0.949	0.820	0.941	0.703
FCoM-me	<u>0.965</u>	<u>0.959</u>	0.934	<u>0.954</u>	0.873	0.942	0.824	0.943	0.738

Table 16: Additional results for different cases of missing views (moderate and extreme) in the **LFMC** data. We highlight the **best** and **second best** value in each scenario. The value in parentheses is the number of available views.

Method	MAPE value (\downarrow)					PRS value (\uparrow)			
	(6/6) No Missing	(5/6) Only missing		(1/6) Only available		(5/6) Only missing		(1/6) Only available	
		Radar	Optical	Optical	Radar	Radar	Optical	Optical	Radar
ITempD-co	<u>0.157</u>	0.293	0.293	0.335	0.335	0.465	0.465	0.433	0.433
ISensD-co	0.191	0.189	<u>0.230</u>	0.249	0.292	0.980	0.819	0.794	0.674
FSensD-cr	0.211	0.221	0.287	0.327	0.377	0.966	0.772	0.727	0.627
FCoMI-co	0.406	0.368	0.333	0.378	0.510	0.999	0.977	0.926	0.793
FEmbr-sa	0.191	0.196	0.265	0.721	0.381	0.964	0.748	0.073	0.381
ESensI-av	0.254	0.276	0.278	<u>0.252</u>	0.283	0.980	<u>0.943</u>	<u>0.911</u>	<u>0.769</u>
FCoM-av	0.173	0.178	0.235	0.907	0.623	0.968	0.791	0.073	0.093
FCoM-ga	0.150	0.156	0.198	0.252	0.297	0.971	0.737	0.608	0.513
FCoM-cr	0.217	0.228	0.250	0.405	0.429	0.920	0.847	0.432	0.383
FCoM-me	0.167	<u>0.165</u>	0.198	0.268	0.299	<u>0.981</u>	0.806	0.685	0.586

Table 17: Additional results for different cases of missing views (moderate and extreme) in the **PM25** data. We highlight the **best** and **second best** value in each scenario. The value in parentheses is the number of available views.

Method	MAPE value (\downarrow)					PRS value (\uparrow)			
	(3/3) No Missing	(2/3) Only missing		(1/3) Only available		(2/3) Only missing		(1/3) Only available	
		Condition	Dynamic	Dynamic	Condition.	Condition	Dynamic	Dynamic	Condition
ITempD-co	0.439	0.439	1.242	1.033	1.594	0.186	0.146	0.185	0.146
ISensD-co	0.879	0.878	1.301	1.151	1.644	0.835	0.690	0.834	0.690
FSensD-cr	1.003	1.149	1.301	1.147	1.300	0.783	0.862	0.757	0.832
FCoMI-co	1.281	0.713	1.088	0.747	1.422	0.994	1.000	0.984	1.000
FEmbr-sa	0.717	0.712	0.976	1.038	1.330	0.933	0.903	0.591	0.693
ESensI-av	0.953	0.754	1.223	0.699	1.561	<u>0.989</u>	0.906	0.991	0.889
FCoM-av	<u>0.581</u>	<u>0.561</u>	2.891	4.957	1.162	0.869	0.408	0.080	0.720
FCoM-ga	0.651	0.658	1.030	<u>0.672</u>	<u>1.051</u>	0.980	<u>0.995</u>	<u>0.996</u>	<u>0.992</u>
FCoM-cr	0.597	0.614	0.728	0.651	0.805	0.949	0.680	0.847	0.701
FCoM-me	0.672	0.653	<u>0.884</u>	0.803	1.318	0.979	0.980	1.000	1.000

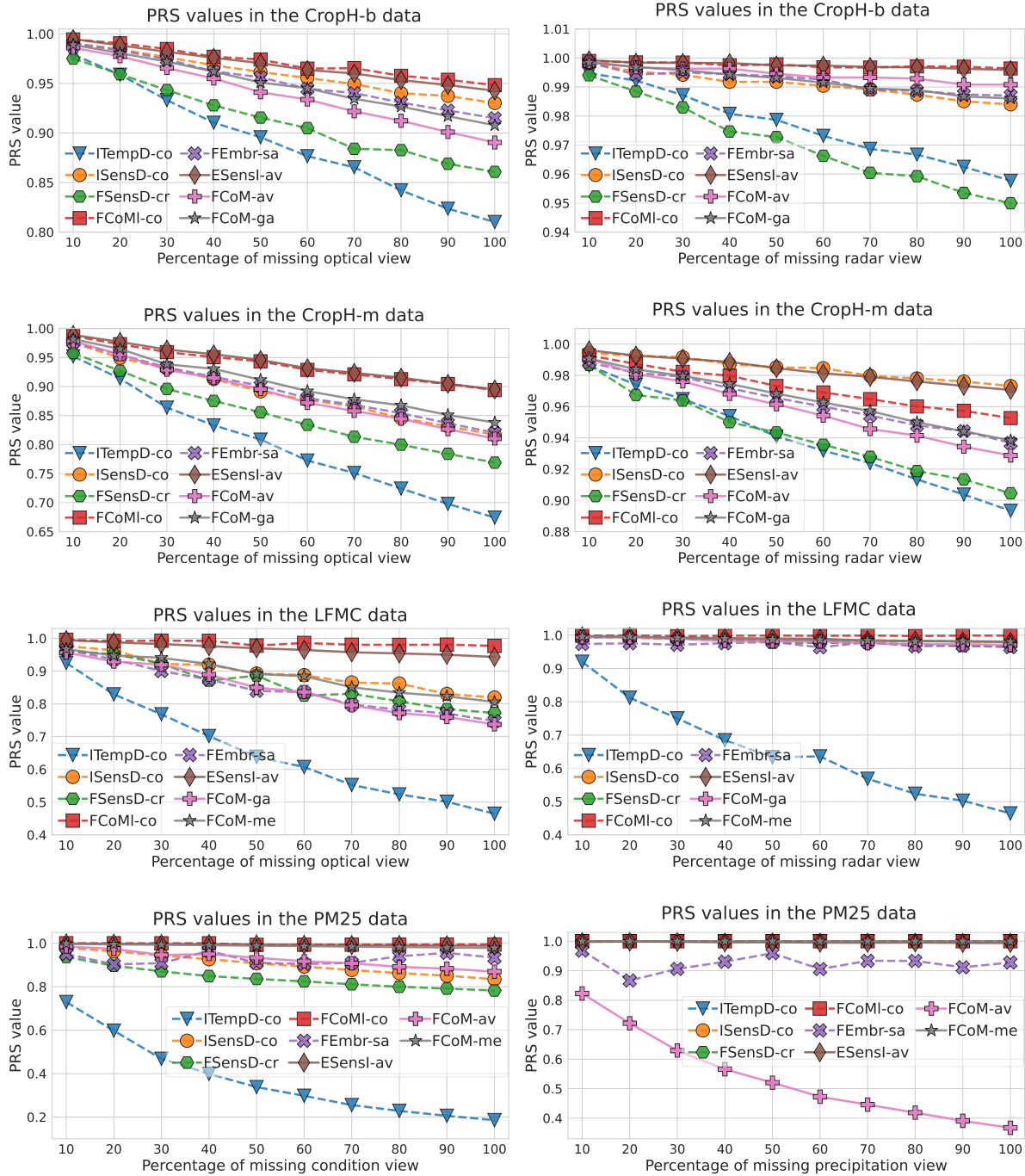


Figure 8: Predictive robustness when the *top* views are missing at different percentages.